# Theoretical investigation of the autoionization process in molecular collision complexes: $He^*(2\,^3S)+Li(2\,^2S)\rightarrow He+Li^+ + e^-$

M. Movre,[a] L. Thiel,[b] and W. Meyer[c]
*Fachbereich Chemie, Universität Kaiserslautern, D-67663 Kaiserslautern, Federal Republic of Germany*

(Received 28 March 2000; accepted 27 April 2000)

A complete *ab initio* treatment is applied to the autoionization process in the $He^*(2s\,^3S)+Li(2s\,^2S)$ collisional complex. Feshbach projection based on orbital occupancy, implemented in a multireference configuration interaction (MRCI) code, defines the resonance state and provides the entrance channel potential curve as well as all pertinent information on the resonance–continuum coupling. The *l*-dependent coupling elements in local approximation are obtained by projecting a compact one-electron function, named Penning molecular orbital (PMO), onto the wave function of the ejected electron with proper energy. The continuum wave function is obtained by coupled channel calculations in the static-exchange approximation. A converged set of seven complex coupling matrix elements, used in the nuclear dynamics calculation based on a complex Numerov algorithm, fully describes the electron angular momentum transfer. The calculated angle-dependent spectra, as well as the total, angle-, and energy-integrated ionization cross sections agree well with available experimental data. © *2000 American Institute of Physics.* [S0021-9606(00)30828-5]

## I. INTRODUCTION

The first complete *ab initio* treatment of Penning (PI) and associative (AI) ionization processes in the $He^*(2s\,^3S)+H(1s)$ collisional complex[1] clearly demonstrated not only the adequacy of the local complex potential approach for this benchmark system, but in particular the importance of electron angular momentum transfer so far neglected in theoretical treatments. We have also argued that the procedures presented provide an adequate treatment for a large class of autoionizing molecular collisional complexes, characterized by core-excited (Feshbach) resonance states as they, e.g., evolve from metastable states of excited rare gas atoms.

The validity range of the local approximation for the treatment of the Penning process (as developed and presented by Nakamura,[2] Miller,[3] and Bieniek[4]) has been discussed by Lam and George[5] and Morgner.[6] The metastable states of rare gas atoms have large excitation energies, which exceed the ionization energy of most atoms (and molecules). During collision, ionization can occur with high probability and electrons are ejected at relatively large energies. This property allows the application of the Born–Oppenheimer approximation for thermal collision energies. Furthermore, because the electronic continuum is unstructured (weak dependence of the coupling on electron energy) and the allowed exit channel nuclear states are complete with respect to the entrance channel wave functions, the ionization can be viewed as a vertical (Franck–Condon) transition. Thus, the entrance channel nuclear motion is governed by a local complex potential. However, even in the local approximation, only few quantitative applications have so far appeared in the literature, all of them being restricted to some of the aspects of the complete theory. (For a comprehensive review of experimental and theoretical research in the field of Penning and associative ionization, see the article by Siska.[7]) The main reason was usually the lack of information on electronic coupling matrix elements between the resonance state and specific final states corresponding to outgoing electrons with angular momentum quantum numbers *l* and *m*. The consequences of the common approximate treatment, which is restricted to $l=0$ and assumes a real coupling matrix element proportional to the square root of the ionization width, have been discussed in Ref. 1.

In Ref. 1 we also gave a detailed description of the *ab initio* computational procedures applied: implementation of Feshbach projection in a multireference configuration interaction (MRCI) code, which defines the resonance state and provides the entrance channel potential curve as well as all pertinent information on the resonance–continuum coupling. This is first compressed into a compact one-electron function, which we named the Penning molecular orbital (PMO) and which represents the source of continuum electrons. This PMO is then expressed in form of a numerical partial wave expansion and is projected onto the wave function of the ejected electron with proper energy, as obtained by coupled-channel calculations in the static-exchange approximation.

We have thoroughly discussed the inherent flexibility in the definition of the Feshbach projection, and subsequently we have proposed two definitions of complementary projection operators *P* and *Q*, both of them in terms of electron configurations. The one named ''resonance procedure'' is based on orbitals optimized for core-excited structures and is most convenient for accurate resonance potentials, and the other, named ''target procedure,'' is based on optimal target orbitals (we use ''target'' in the sense of electron scattering in the exit channel system, here $HeLi^+$) and is adapted to the

[a]Permanent address: Institute of Physics, Universite of Zagreb, HR-10000 Zagreb, Croatia.
[b]Permanent address: FB Physik, Universität Kaiserslautern, Germany.
[c]Electronic mail: meyer@chemie.uni-kl.de

 

simplest possible description of the exit channel electronic states. This difference is not a trivial one, due to significant relaxation effects in the noble gas cores which accompany the creation of a hole. For example, the $1s$ orbital of He contracts upon excitation according to the change of the orbital exponent from 1.7 to 2.0, yielding a relaxation energy of about 1 eV. Consequently, the resulting PMOs are not necessarily the same in the two procedures. However, after being projected onto the energy shell both of them yield basically the same coupling matrix elements. [We have shown that for atomic $(1s2s^2)\,^2S$ resonances of Li and $He^-$, both procedures lead to equivalent results—for further details see Ref. 1.] In the $He^*(^3S)+H$ case, we have also analyzed the dependence of the width function on the electron energy for several fixed internuclear separations. It turned out that the shape of the width function does depend on the definition of the $P$ and $Q$ operators but the value of the width function for electron energies close to the resonance energy stays rather stable.

With the derivation of complex $l$-dependent coupling matrix elements we have the complete electronic structure input for the subsequent treatment of nuclear motion and the calculation of angle-dependent electron energy distributions. These coupling matrix elements are directly linked to the internal angular distribution of the electrons, and the interplay of their phases with those acquired in the heavy particle motion determines the dependence of the electron spectra on the detection angle.

In this article we present the results of theoretical investigations of the attractive Penning system $He^*(2s\,^3S)+Li$, one of the few simple systems for which well-resolved electron energy spectra have been measured, also including information on their angular dependence.[8,9] Our previous efforts[9,10] for a theoretical analysis and a reliable calculation of autoionization electron spectra for this system were directed towards an accurate adiabatic potential of the resonance state. The total width function was obtained by Stieltjes imaging[11,12] with an estimated accuracy of 10%. These data were used for the calculation of the nuclear dynamics in the commonly used approximation (see Ref. 1 for discussion) which neglects angular momentum transfer and provides electron energy spectra in best agreement with measurements based on electron detection perpendicular to the collision plane. In order to illustrate the anticipated effects of angular momentum transfer, we also calculated approximate spectra simply assuming pure $\Delta J=\pm 4$ transitions. We are not aware of any other previous calculations for the He*+Li system.

## II. BASICS OF THEORY

Two complementary projection operators $P$ and $Q=1-P$ partition the electronic Hilbert space into two subspaces, one containing the relevant ''background'' continuum states and the other containing the ''bound,'' resonance, or autoionizing state(s). The continuum states describe asymptotically the ground state of the ionized molecular complex and a free electron ejected with energy $\varepsilon$ in the space-fixed direction $\hat{\omega}r(\vec{\varepsilon}=\varepsilon\hat{\omega})$. The corresponding electronic wave function behaves asymptotically as the product of the ground state wave function of the ionized complex and a free electron wave function, $\phi_{\vec{\varepsilon}}\rightarrow\Phi_+\varphi_{\vec{\varepsilon}}$, while the resonance state is described by an electronic function $\phi_*$. The entrance channel (resonance) potential $V_*(R)$, the exit channel potential $V_+(R)$, and the PMO $\varphi_P$ are defined as $V_*=\langle\phi_*|H_{\rm el}|\phi_*\rangle$, $V_+=\langle\Phi_+|H_{\rm el}|\Phi_+\rangle$, and $\varphi_P=\langle\Phi_+|H_{\rm el}|\phi_*\rangle$, respectively, where $H_{\rm el}$ is the electronic Hamiltonian. The continuum electronic wave function is further assumed in the form

$$\phi_{\vec{\varepsilon}}=\hat{A}\Phi_+\varphi_{\vec{\varepsilon}}=\hat{A}\Phi_+\sum_{lm} i^l Y^*_{lm}(\hat{\omega}_{\hat{R}})\varphi_{\varepsilon lm}(\vec{r}_{\hat{R}}), \tag{1}$$

where $\hat{A}$ antisymmetrizes the product of $\Phi_+$ with the continuum electron wave function. Note that the partial waves refer to the molecule-fixed coordinate system, as indicated by the subscript $\hat{R}$ on $\hat{\omega}$ and $\vec{r}$, in which $m=0$ is a good quantum number in our case.

The continuum electron moves in an anisotropic potential and its wave function should further be expanded as

$$\varphi_{\varepsilon lm}(\vec{r}_{\hat{R}})=\sum_{l'} Y_{l'm}(\hat{r}_{\hat{R}})f_{\varepsilon ll'}(r)r^{-1}, \tag{2}$$

where asymptotically $f_{\varepsilon ll'}\rightarrow 0$ for $l\neq l'$. Note that in Bieniek's[4] and previous treatments the right-hand side of Eq. (2) was reduced to a single term $l'=l$, supposing a pure Coulomb wave. The phase shift pertinent to the radial function $f_{\varepsilon ll}$ comprises not only the Coulomb phase shift in a field of unit positive charge at $Li^+$ but also a contribution due to the atomic potentials of He and $Li^+$.

The basic quantities required for the calculation of various cross sections are complex partial wave components $V_{\varepsilon l}$ related to the space-fixed coupling matrix elements $V_{\vec{\varepsilon}}(\vec{R})$ by

$$V_{\vec{\varepsilon}}(\vec{R})=\langle\phi_{\vec{\varepsilon}}|H_{\rm el}|\phi_*\rangle=\sum_l i^{-l}Y_{lm}(\hat{\omega}_{\hat{R}})V_{\varepsilon l}(R). \tag{3}$$

Within our approach they reduce to simple overlap integrals $V_{\varepsilon l}=\langle\varphi_{\varepsilon l}|\varphi_P\rangle$.

The total (electronic and nuclear) wave function is of the form $\psi_E=P\psi_E+Q\psi_E$, and can be obtained as the solution of a pair of coupled equations for the two components (for more details, see Ref. 1). The $Q$-space part (entrance channel) of the scattering solution with proper outgoing boundary conditions is, in the case of an isolated resonance, a single (Born–Oppenheimer) product of the electronic wave function and a nuclear wave function, $Q|\psi_E^{\rm out}\rangle=|\phi_*\rangle|\chi_*^{\rm out}\rangle$. Similarly, the solution of the corresponding homogeneous equation in the exit channel is $P|\psi_E^0\rangle=|\phi_{\vec{\varepsilon}}\rangle|\chi_{\vec{E}_+}\rangle$, where $E_++\varepsilon=E$, and $\vec{E}_+=E_+\Omega_+$ denotes the energy and asymptotic direction of the motion of the ionized complex ($He+Li^+$ for PI, and $HeLi^+$ for AI). The scattering nuclear wave functions are usually expanded into partial waves composed of the products of angular and radial wave function. The radial wave function of the exit channel $F^+_{J'}$ obeys the radial Schrödinger equation for the potential $V_+$, while the entrance-channel radial wave function $F_J$ obeys the radial

Schrödinger equation for the complex potential $V_*+\Delta-(i/2)\Gamma$, where the local width $\Gamma(R)$ and the local shift $\Delta(R)$ are finally given as

$$\Gamma(R)=2\pi\int d\hat{\omega}|V_{\vec{\varepsilon}}(\vec{R})|^2|_{\varepsilon=\varepsilon_v(R)}, \tag{4}$$

$$\Delta(R)=\mathcal{P}\int d\vec{\varepsilon}'\frac{|V_{\vec{\varepsilon}'}(\vec{R})|^2}{\varepsilon_v(R)-\varepsilon'}, \tag{5}$$

where $\varepsilon_v=\varepsilon(R_v)=V_*(R_v)-V_+(R_v)$ (vertical Franck–Condon transition).

The double differential cross section which describes the energy and angle distribution of the ejected electron is given by

$$\frac{d^2\sigma}{d\varepsilon\, d\hat{\omega}}=g_*\frac{4\pi^3}{k_i^2}\sum_{J'M}\left|\sum_{Jl}\begin{pmatrix} J' & l & J\\ -M & M & 0\end{pmatrix}\times Y_{lM}(\hat{\omega})C_{J'lJ}\langle F^+_{J'}|V_l|F_J\rangle\right|^2, \tag{6}$$

where

$$C_{J'lJ}=i^{J-J'-l}(2J'+1)^{1/2}(2J+1)\begin{pmatrix} J' & l & J\\ 0 & 0 & 0\end{pmatrix}. \tag{7}$$

## III. DETAILS OF CALCULATIONS

The exit channel electronic state of $HeLi^+$ is a singlet state, so that only doublet $^2\Sigma^+$ states of He*Li are autoionizing. The core electrons of Li can be treated as essentially unaffected in the course of the PI process since core excitations are not accessible energetically. (The same is true for Na, while in the case of K and Rb core excitation energies are comparable to the excitation energy for He*, so that complications arise from core-excited alkali states.[13]) Treating $Li^+$ as a polarizable core, we have performed all-electron self-consistent field (SCF)/valence configuration interaction (CI) calculations, using the technique of multireference self-consistent electron pairs (MRSCEP)[14,15] and we included core polarization effects by an effective local potential.[16]

The electronic structure of the resonance state correlated to the $He^*(2s\,^3S)+Li(2s\,^2S)$ asymptote undergoes significant changes as the interatomic distance varies. At short distances it is well-described by the single configuration $(core)1\sigma(2\sigma)^2$. The orbital $2\sigma$ is dominantly a covalent combination of the He $2s$ and the Li $2s$ atomic orbitals. (In the case of He*H, it represents a dominantly $H^-$ $1s$ atomic orbital, see Ref. 1.) At intermediate distances, the configurations $1\sigma(3\sigma)^2$ and $1\sigma(2\sigma3\sigma)$ with an antibonding delocalized $3\sigma$ orbital gain significant weight. The asymptotic state is described by these three configurations with relative weights 3:3:2, respectively. Due to the large polarizability of He* at intermediate ranges there are also significant admixtures by the He $2p_\sigma$ orbital, in particular for the state correlating to $He^*(2s\,^1S)+Li(2\,^2S)$. Therefore, we started our calculations by using multiconfiguration SCF (MCSCF) wave functions optimized in the space of the $14\,^2\Sigma^+$ configurations which are possible from the six ''active'' orbitals $1\sigma-4\sigma,1\pi_x,1\pi_y$ under the condition that $1\sigma$ is at least singly-occupied. The $1\sigma$ orbital has been taken from a preceding SCF calculation for the cation $LiHe^+$ and kept frozen (target procedure). This ansatz provides an adequate description of the four asymptotes correlating to He* $^{1,3}S$ and $^{1,3}P$, respectively.

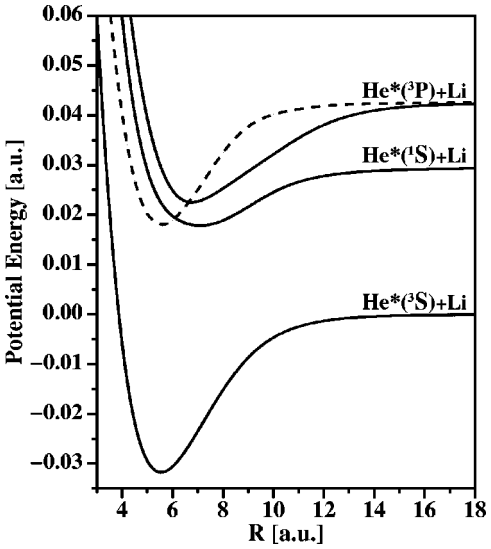


FIG. 1. Calculated potential energy curves of three lower $^2\Sigma^+$ states (solid lines) and one $^2\Pi$ state (dashed line) corresponding to the asymptotic states $He^*(^3S,\,^1S,\,^3P)+Li$.

The partitioning of the electronic Hilbert space into two complementary subspaces was achieved by defining projection operators $Q$ and $P=1-Q$ in the following manner (for further details, see Ref. 1): The $Q$ space for the final CI was generated by all single and double substitutions from the 14 reference configurations, excluding the configurations of the type $(core)(1\sigma)^2n\sigma$ with $n>4$. For $n\leqslant 4$, the latter configurations correlate to the few lowest excited (Rydberg) states He+Li* and do not belong to the exit channel. As in the He*+H case,[1] they do not contribute much to the resonance states either.

The Gaussian basis set used in our calculation is composed as follows. For He we used the 10$s$ set of Ref. 17 augmented with 3$s$ (exponents 0.04, 0.016, 0.0064), a 5$p$ set (3.0, 0.9, 0.3, 0.08, 0.025), and 1$d$ set (0.08). For Li we used the 9$s$ set of Ref. 18 with the two most diffuse functions replaced by 3$s$ (0.13, 0.055, 0.022), 6$p$ (2.0, 0.63, 0.24, 0.1, 0.04, 0.016), and 1$d$ (0.12). The steepest functions—5$s$ for He and 4$s$ for Li—have been contracted according to their coefficients in an uncontracted calculation. In order to get a faster convergence for the correlation in the valence shell, which shows a rather strong electron accumulation around the bond center, we have included some additional functions at the bond center (for further details, see Refs. 19 and 20).

## IV. RESULTS

### A. Potential curves

The four calculated potentials (three $^2\Sigma^+$ and one $^2\Pi$) are shown in Fig. 1 (numerical data are available upon request). The accuracy of our calculations may be judged from

previous $Li_2$ calculations[19,20] by the same method and a similar basis set, in which case the experimental well depth of $D_e=1.056$ eV has been reproduced to within 6 meV. Thus, we roughly estimate that our calculated values are correct to within 10 meV. For the $^2\Sigma^+$ He*$(2s\,^3S)$+Li potential, we have calculated a well depth of $D_e=867$ meV and an equilibrium distance of $R_e=5.54\,a_0$. This may be compared with the empirical values of $D_e=868(20)$ meV and $R_e=5.4(3)\,a_0$, respectively, extracted from observed electron energy spectra.[8] For the $^2\Sigma^+$ He*$(2s\,^1S)$+Li potential the calculated values are $D_e=315$ meV and $R_e=7.06\,a_0$ while the corresponding empirical values are $D_e=330(17)$ meV and $R_e=6.9(8)\,a_0$, respectively.[8] Thus, our calculated values match the experimental ones within their quoted errors. We note that in a second experimental study of He* and Li collisions using the merged-beams technique a well depth of 730(70) meV has been derived from analysis of the kinetic energy distribution of the product ion.[21] The difference can probably be traced to the fact that in this case the two entrance channels from asymptotic He*$(2s\,^3S)$ and He*$(2s\,^1S)$ atoms could not be distinguished.

It has often been noted that in many respects metastable noble gas atoms behave like alkali atoms, in particular He*$(2s\,^3S)$ has been called lithiumlike.[8] Actually, comparing some atomic properties of Li, Na, K, and He*$(^3S)$, for example ionization energies, first resonance transition energies, or atomic polarizabilities, as well as well depths and equilibrium distances for the corresponding diatomic pairs, one can conclude that in almost all respects He*$(^3S)$ comes closer to Na. Of course, an obvious difference between He*$(2s\,^3S)$ and the alkalis is the presence of the open-shell core, and the exchange interaction with the $2s$ electron is in the same order-of-magnitude as the chemical interaction in the valence shell. Thus it is only accidental that the He*$(^3S)$Li potential is virtually identical to the NaLi ground state potential.[19]

### B. Coupling elements

For systems such as He*+Li, Na, electrons of energies around 13 eV (that is, with de Broglie wavelengths of about $6\,a_0$) are ejected mainly from a region close to the He $1s$ core and then move in a Coulomb field that is centered $4-10\,a_0$ away, thus requiring the coupling of many electron angular momenta in the expansion of the wave functions $\varphi_{\varepsilon l}$ of the ejected electron, Eq. (2). They are derived in numerical form in the static-exchange approximation with $\varphi_{\varepsilon l}$ chosen orthogonal to all orbitals occupied in the ground state wave function of the ionized complex (for more details, see Ref. 1). With He as the expansion center, on average 16 coupled angular momenta $l'$ [see Eq. (2)] were required to obtain well-converged results for the complex coupling matrix elements $V_{\varepsilon l}=\langle\varphi_{\varepsilon l}|\varphi_P\rangle$. The final $l$-dependent coupling matrix elements, referring to the center of mass as origin, are shown in Fig. 2 for $l=0-5$ and a set of internuclear separations starting at $R=3.5\,a_0$. Note that the most efficient region for ionization in thermal collisions involves the points 2–6 corresponding to internuclear distances $R$ from 4 to $6\,a_0$. Except for a peculiar behavior of the $l=0$ curve for very small $R$, the main pattern of characteristic spiral curves are similar to the ones obtained for the He*$(^3S)$+H case. The strong decrease of the norms with increasing internuclear distances is basically exponential and is the expected consequence of the exchange mechanism for ionization. The corresponding phase changes are partly due to the changes of the electron resonance energy with $R$. The total width $\Gamma$, together with the partial widths $\Gamma_l=2\pi|V_l|^2$ $(l=0-5)$, is shown in Fig. 3. At shorter distances up to about $3.8\,a_0$ the $l=2$ component is the dominant one with significant contributions from the $l=1$ and 3 components. The latter takes over for intermediate distances while the $l=4$ component becomes dominant for $R>6\,a_0$.

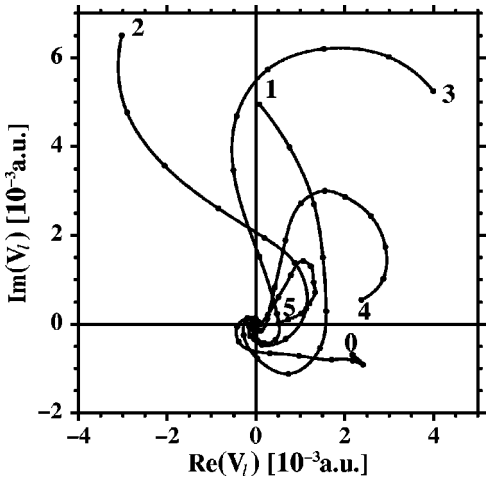


FIG. 2. Complex coupling elements $V_l(R)$ (in a.u.). The internuclear distances are indicated by dots, starting with $R=3.5\,a_0$ at the point labeled by $l$, and continuing in steps of $0.5\,a_0(3.5\,a_0-6.0\,a_0)$ and $1\,a_0(6\,a_0-12\,a_0)$. The most efficient region for ionization in thermal collisions involves the points 2–6.

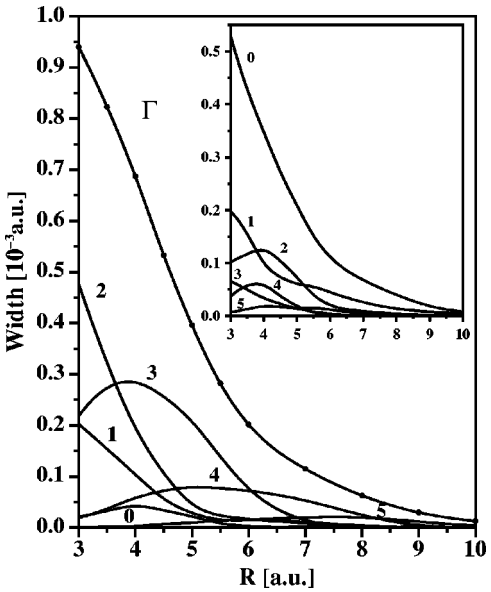


FIG. 3. Partial width functions $\Gamma_l=2\pi|V_l(R)|^2$ for $l=0-5$, referring to the center-of-mass as origin, and the total width function $\Gamma=\Sigma_l\Gamma_l$. Inset: partial width functions $\Gamma_l$ referring to He as the expansion center.

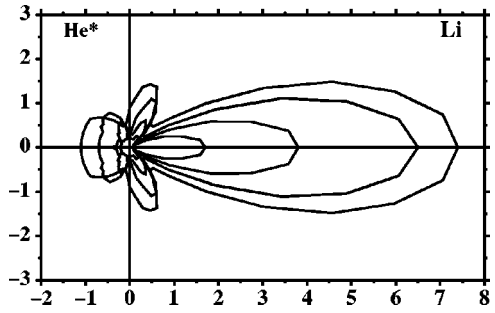


FIG. 4. Internal angular distribution $P_{\mathrm{int}}(\theta,R)$ of the electrons ejected from the collision complex He*$(2\,^3S)$+Li. The parameter $R$ is varied from $R=3\,a_0$ (outer curve) to $R=6\,a_0$ (inner curve) in steps of $\Delta R=1\,a_0$. The intensity scale of the polar plot is proportional to the autoionization width $\Gamma(R)/2\pi$ (a.u.).

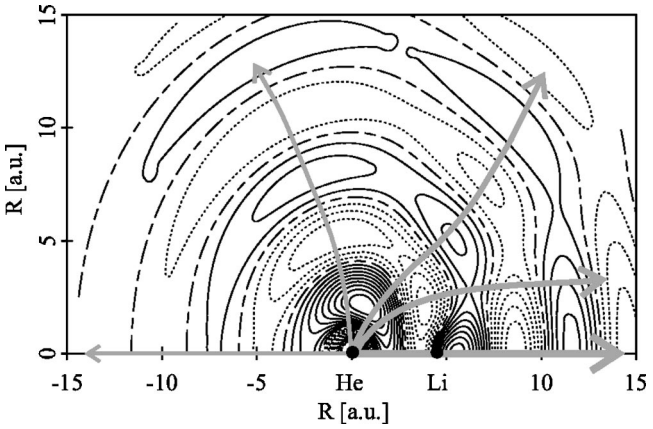


FIG. 5. Wave function of the ejected electron for $R=4.5\,a_0$. The gray arrows indicate the electron flux.

The $l$-distribution of the coupling matrix elements suggests a significant angular momentum exchange, dominated by $|\Delta J|=3$ and 4 for distances $4\,a_0<R<6\,a_0$. Due to the fact that the entrance channel turning point is rather large $(\sim 4\,a_0)$ and the center-of-mass is close to $Li^+$, a simple classical estimate based on recoil arguments led Merz *et al.*[9] to the conclusion that $|\Delta J|$ values up to $l_{\max}=4$ are possible.

### C. Internal angular distribution

The classical description of the angular distribution of ejected electrons is often based on the analysis in terms of the intrinsically unmeasurable internal angular distribution.[7] For a specific internuclear separation $R$, it is given by

$$P_{\mathrm{int}}(\theta,R)=|V_{\vec{\varepsilon}_v}(\vec{R})|^2=\left|\sum_l i^{-l}V_l(R)Y_{lm}(\theta,0)\right|^2, \qquad (8)$$

where $\theta$ represents the body-fixed electron scattering angle. Figure 4 shows the *ab initio* internal angular distribution for several internuclear separations $R$. The general pattern of anisotropy and asymmetry remains the same for all $R$. Even though the overall internal angular distribution requires integration over $R$, collision energies $E_{\mathrm{rel}}$, and impact parameters $b$, it should not be significantly different from the shapes given in Fig. 4. There is a pronounced asymmetry in forward–backward direction and a small but sharp maximum near the perpendicular direction.

By expanding the absolute square one can transform Eq. (8) into a form that is more convenient for the analysis of angular dependence:

$$P_{\mathrm{int}}(\theta,R)=\sum_{Lll'} a_L(l,l')P_L(\cos\theta)\begin{pmatrix} l' & l & L \\ 0 & 0 & 0 \end{pmatrix}. \qquad (9)$$

The parity of the Legendre polynomials is $(-1)^L$ and it is clear that only odd $L$ terms contribute to the forward–backward asymmetry. The 3-$j$ symbol is unequal to zero only if $l+l'+L=$even, and it follows that for $L$ to be odd, there must be both even and odd $l$ terms in expansion (3). Although the $l$-expansion of the coupling matrix element in the center-of-mass frame is quite different from the corresponding expansion centered at the He atom (see Fig. 3), the resulting internal angular distribution remains unchanged. For example, a single-term $l=0$ expansion in the latter case would produce an isotropic internal angular distribution as would the expansion with respect to a shifted center; even so, the latter one produces all possible $l$. The observed asymmetry is a consequence of the intrinsic underlying asymmetry in the electronic structure of the wave function describing the ejected electron. To illustrate this point further we show in Fig. 5 the wave function of the ejected electron for $R=4.5\,a_0$. With a bit of imagination, using the contour lines and gradients (orthogonal to the contour lines) as a guide, one can judge how the (asymptotic) internal angular distribution evolves. One can identify forward–backward asymmetry, as well as lateral maxima, and even visualize the focusing effect of the Coulomb center at Li for the electrons which are ejected mainly from the vicinity of the He 1$s$ hole. To this end we have added a few (gray) arrows which indicate the main electron flux.

### D. The energy dependence of the electron spectra

The general structure of the electron spectra is easily related to the characteristic properties of the attractive Penning system, and the gross structure of the Penning part can be well explained by a semiclassical treatment.[3,4,22] The spectrum stretches over more than 1 eV and comprises contributions from nuclear angular momenta $J$ ranging up to about 80 for a typical thermal collision energy of 100 meV. The variation of the spectral shape with collision energy $E_{\mathrm{rel}}$ is mainly due to the change of the range of contributing angular momenta $J$. Once the sum over $J$ is made, the interference patterns pronounced in individual $J$ contributions to the spectrum are progressively washed out with increasing collision energy $E_{\mathrm{rel}}$. The PI part of the spectrum ($\varepsilon<\varepsilon_0$, where the ''nominal'' energy $\varepsilon_0$ is the energy at which an electron would be emitted in the separated atom limit) exhibits the familiar Airy pattern with a supernumerary rainbow structure connected with the minimum in the difference potential $V_*-V_+$. The main Airy peak is built up mainly from high-$J$ contributions. The weak AI part of the spectrum ($\varepsilon \geqslant \varepsilon_0$) is mainly linked to low-$J$ values and the turning point region of the entrance potential. The shape of the AI spectrum is rather insensitive to the shape of the width function.

We have calculated the energy-dependent total ionization as well as the associative ionization cross section, and the cross section for long-lived resonance states. For $E_{rel} < 300$ meV the energy dependence of the calculated total ionization cross section is well-described by $\sigma(E) = CE^{-0.325}$, where $C = 16.04$ if cross sections are in Å$^2$ and energies in eV. This is in agreement with the expectation that for attractive systems the total cross section should be proportional to the orbiting, or close-collision cross section, which for the van der Waals long-range potential follows a $E^{-1/3}$ dependence. Wang *et al.*[21] reported a $E^{-0.34}$ dependence. Within the stated uncertainty of ±30%, their absolute cross sections are also compatible with our calculations. The calculated AI cross sections are less than 1.5% of the corresponding total cross sections and the contribution of the long-lived resonances to the total cross section is negligible, again in accordance to findings of Wang *et al.*[21]

### E. The angle dependence of the electron spectra

For use in the dynamics calculations [Eq. (6)], the *ab initio* calculated coupling matrix elements need to refer to a partial-wave expansion with respect to the center-of-mass as origin. In connection with the emission of nonspherical partial electronic waves, $l > 0$, all transitions of the molecular rotation with $|\Delta J| \leq l$ are possible. For the most efficient internuclear distances around $4.5\,a_0$ the leading partial width contribution is $l = 3$, followed by significant contributions from $l = 2,4$, and small terms from $l = 0,1$ (see Fig. 3). As stated, there is a sizable angular momentum transfer to the emitted electron with $|\Delta J|$ up to 4.

Spectral features that are specifically related to the electron emission angle are best demonstrated on the basis of spectra for single collision energies. Theoretical angle-dependent electron spectra for a single collision energy of $E_{rel} = 100$ meV are shown in Fig. 6. The spectra are shown with an electron energy resolution of 10 meV. At that level, the rotational structure is smeared out, but there is a lot of interference structure left. There is a significant difference in the structure and modulation in the Penning part as well as in the associative part of the spectrum. The modulation is more pronounced in forward and backward direction than at 90°. The main Airy peak is shifted towards lower energies when going from 0° (forward) to 180° (backward) direction. Changes in the modulation of the main peak, as well as shifts of the secondary Airy peaks, are also clearly visible. So far, the description of the angular dependence of the electron spectra parallels the one for the He*H case.[1] But there is also a difference in the two cases caused by the different composition of the partial width expansion. This difference is more clearly visible in the internal angular distribution. While in the He*H case, the internal angular distribution exhibits similar maxima in the backward and forward direction, this is not the case for the He*Li collisional system. This difference, as stressed by the fact that $l = 2$ dominates the partial-wave expansion for He*H, while $l = 3$ is the leading term in the case of He*Li, could be traced back to the difference in the electronic structure of the resonance states, respectively. [At the most relevant interatomic distances, the lowest resonance state for both systems is well-described by the single configuration $1\sigma(2\sigma)^2$, but the orbital $2\sigma$ is dominated by the $H^-1s$ component in the case of He*H, while in the case of He*Li it is dominantly a covalent combination of the He $2s$ and the Li $2s$ atomic orbitals.]

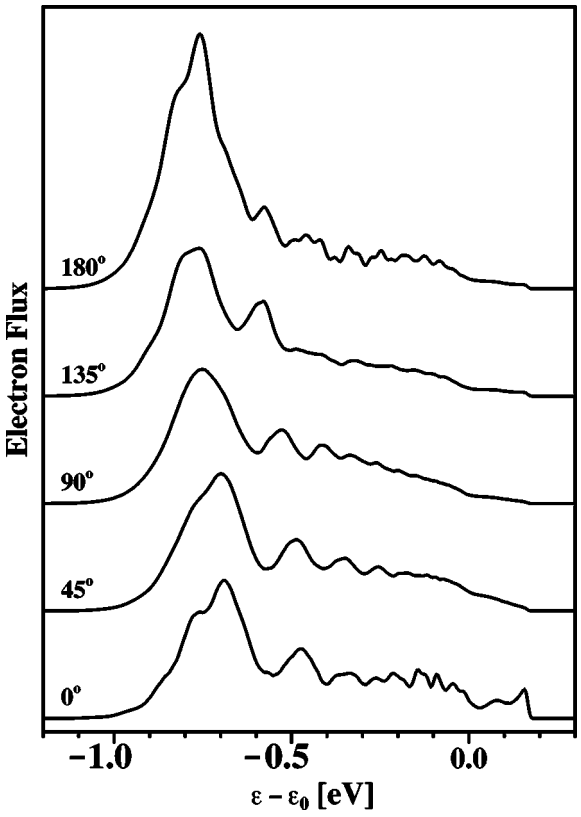


FIG. 6. Calculated electron energy spectra at different detection angles $\theta$ for a single collision energy $E_{rel} = 100$ meV and an electron energy resolution of 10 meV. The electron energy is defined relative to the ''nominal'' energy $\varepsilon_0$ at which an electron would be emitted in the separated atom limit. One can see substantial angular dependence of the electron spectra for He*($^3S$) + Li.

A substantial angular dependence of the electron energy spectra for He*Li was reported by Merz *et al.*[9,10] Although the observed spectra were heavily averaged over the range of angles (up to ±25° for $\theta = 90°$), the following changes in the electron spectra were reported: (i) energy shifts of the Airy interference structure to higher electron energy with decreasing emission angle $\theta$, (ii) difference in the clarity, with which the structure is observed, for varying $\theta$, (iii) a relative increase in the intensity of the plateau, observed towards higher energies, with decreasing angle $\theta$.

We did not try to reproduce the experimental results of Merz *et al.*[9,10] by a direct simulation of the experimental conditions because of lack of precise knowledge of the velocity distributions of the two atomic beams. It should be noted that these experiments were the first to establish an angular dependence in the electron spectra for an attractive Penning system for which usually isotropy has been assumed. Prior to the development of a new apparatus, as used in the later He*H experiments,[23] the apparatus had to be opened between measurements at different detection angles and uncontrollable changes in the experimental conditions cannot be excluded.[24] Instead, we show in Fig. 7 the simu-

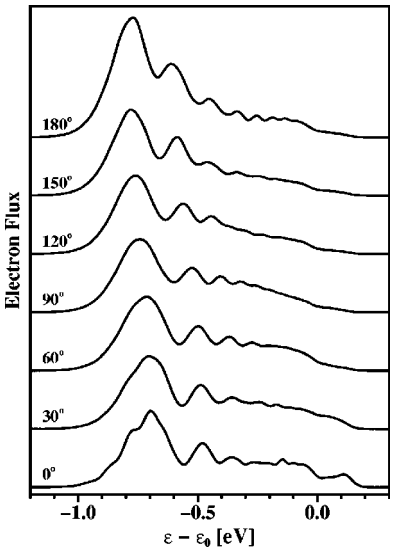


FIG. 7. Calculated electron spectra for an in-plane variation of the detection angle $\theta$. The spectra correspond to a quasithermal collision energy with a mean value of 100 meV (see text for details) and a resolution of 25 meV.

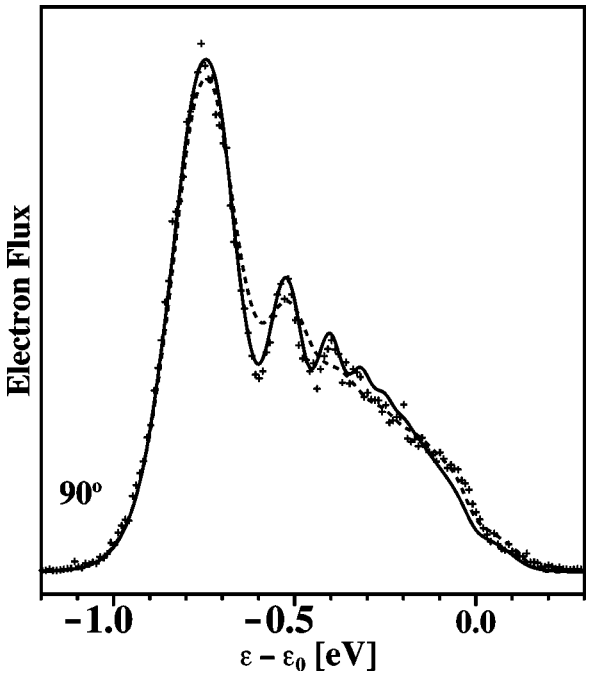


FIG. 8. Measured (+) (Ref. 8) and calculated (solid line) electron spectrum for detection at 90° perpendicular to the plane of the atomic beams, as compared to the calculated angle-integrated spectrum (dashed line). The calculation assumes an electron energy resolution of 35 meV. The spectra are normalized to the same integral value.

lation of electron spectra for a model experimental setup with an in-plane variation of $\theta$, corresponding to the following typical beam parameters: well collimated metastable $He^*(^3S)$ beam with a central velocity of $u=1650$ m/s and an effective temperature of $T=26$ K, and an effusive source of Li atoms with a Maxwellian velocity distribution corresponding to a temperature of $T=1100$ K. These spectra, corresponding to a mean relative collision energy of 100 meV and an electron energy resolution of 25 meV, indeed reproduce all features observed in the experiments. In particular, the shifts of the main Airy peak and the first supernumerary peak agree even quantitatively: between the spectra for 45° and 135°, respectively, the former is shifted by about 60 meV in both cases while the latter is shifted by 90 meV in the calculated spectrum and 110 meV in the experiment.

The measurements of Ruf *et al.*[8] where performed at 90° perpendicular to the plane of the atomic beams with beam conditions close to those given above. As discussed in Ref. 1, the 90° perpendicular spectrum is not influenced by forward–backward asymmetry and most closely resembles a spectrum calculated by the approximate treatment generally used in previous work[7] and also in our previous treatments of He*Li.[9,10] While good overall agreement between the ''approximate'' and the experimental spectrum was achieved, the low energy tail of the main Airy peak was not reproduced quite well. In Fig. 8 we compare the experimental spectrum obtained by Ruf *et al.*[8] with our angle-dependent spectrum as calculated for 90° perpendicular to the collision plane and an electron energy resolution of 35 meV. The resolution chosen corresponds to the quoted nominal resolution of the experiment and not to the estimated one of 60 meV.[8] The calculated spectrum with a 60 meV resolution (not shown in the figure) is clearly too broad and we consider the 60 meV estimate as a very conservative one. The agreement in the region of the main Airy peak is now much better. There is still some discrepancy left for energies just below the nominal energy. This is probably due to the high sensitivity of this part of the spectrum to details of the tails of the interaction potential as well as the width function. Figure 8 also gives the angle-integrated spectrum which is significantly less modulated due to the average over angle-dependent peak positions.

## V. CONCLUSIONS

We have presented new theoretical results for the autoionizing molecular collision complex $He^*(2s\,^3S)+Li(2s\,^2S)$. The Feshbach projection method is used to define the core-excited resonance state and to obtain the corresponding entrance channel potential energy curve as well as all the information needed for the resonance–continuum coupling via the Penning MO. The PMO is then expanded in terms of the solutions of the electron scattering problem in the exit channel, which were obtained by coupled-channel calculations in the static-exchange approximation. Considering the autoionization process as a vertical transition leads to a local complex potential for the resonance state dynamics and local complex coupling elements to continuum states, which correlate asymptotically to electrons of particular angular momentum. Our calculations for the system $He^*+Li$ demonstrate a significant angular momentum transfer to the emitted electron, which is dominated by $|\Delta J|=3$ and 4 for distances belonging to the most efficient region for ionization in thermal collisions. The coupling matrix elements are directly linked to the internal angular distribution of the electrons, and the interplay of their phases with those acquired in the heavy particle motion determines the dependence of electron spectra on the detection angle. We have calculated angle-dependent electron spectra as well as collision-energy-

dependent total ionization cross sections and compared them with available experimental results. We found good agreement between theory and experiment within the experimental uncertainties. The comparison has shown that a purely *ab initio* treatment is capable of calculating reliable electron spectra.

## ACKNOWLEDGMENT

This work has been supported by the Deutsche Forschungsgemeinschaft (Forschergruppe Niederenergetische Elektronenstreuprozesse).

[1] M. Movre and W. Meyer, J. Chem. Phys. **106**, 7139 (1997).
[2] H. Nakamura, J. Phys. Soc. Jpn. **26**, 1473 (1969).
[3] W. H. Miller, J. Chem. Phys. **52**, 3563 (1970).
[4] R. J. Bieniek, Phys. Rev. A **18**, 392 (1978).
[5] K.-S. Lam and T. F. George, Phys. Rev. A **29**, 492 (1984).
[6] H. Morgner, Chem. Phys. **145**, 239 (1990).
[7] P. E. Siska, Rev. Mod. Phys. **65**, 337 (1993).
[8] M.-W. Ruf, A. J. Yencha, and H. Hotop, Z. Phys. D: At., Mol. Clusters **5**, 9 (1987).
[9] A. Merz, M. W. Müller, M.-W. Ruf, H. Hotop, W. Meyer, and M. Movre, Chem. Phys. Lett. **160**, 377 (1989).
[10] A. Merz, M. W. Müller, M.-W. Ruf, H. Hotop, W. Meyer, and M. Movre, Chem. Phys. **145**, 219 (1990).
[11] P. W. Langhoff, Int. J. Quantum Chem., Symp. **8**, 347 (1974).
[12] A. U. Hazi, J. Phys. B **11**, L259 (1978).
[13] C. E. Johnson, C. A. Tipton, and H. G. Robinson, J. Phys. B **11**, 927 (1978).
[14] W. Meyer, J. Chem. Phys. **64**, 2901 (1976).
[15] H.-J. Werner and E.-A. Reinsch, J. Chem. Phys. **76**, 3144 (1982).
[16] W. Müller, J. Flesh, and W. Meyer, J. Chem. Phys. **80**, 3297 (1984).
[17] S. Huzinaga, J. Chem. Phys. **42**, 1293 (1965).
[18] S. Huzinaga, technical report: *Approximate Atomic Functions I and II*, Division of Theoretical Chemistry, University of Alberta, 1971 (unpublished).
[19] I. Schmidt-Mink, W. Müller, and W. Meyer, Chem. Phys. Lett. **112**, 120 (1984).
[20] I. Schmidt-Mink, W. Müller, and W. Meyer, Chem. Phys. **92**, 263 (1985).
[21] D. P. Wang, S. Y. Tang, and R. H. Neynaber, J. Phys. B **20**, 1527 (1987).
[22] R. J. Bieniek, M. W. Müller, and M. Movre, J. Phys. B **23**, 4521 (1990).
[23] A. Merz, M.-W. Ruf, and H. Hotop, Phys. Rev. Lett. **69**, 3467 (1992).
[24] A. Merz, M. W. Müller, M.-W. Ruf, and H. Hotop (private communication).